The Impact of Spatial–Temporal Averaging on the Dynamic–Statistical Properties of Rain Fields

Guangguang Yang, David L. Ndzi, Boris Christian Gremont, Kevin Paulson, Misha Filip, and Abdul-Hadi Al-Hassani

Abstract— Knowledge of the spatial–temporal variation of rain fields is required for the planning and optimization of wide-area high-frequency terrestrial and satellite communication networks. This article presents data and a method for characterizing multi-resolution statistical/dynamic parameters describing the spatial–temporal variation of rain fields across ocean climate in North-Western Europe. The data are derived from the NIMROD network of rain radars. The characterizing parameters include 1) statistical distribution of point 1 min rainfall rates, 2) spatial and temporal correlation functions of rainfall rate, and 3) the probability of rain/no rain. The main contributions of this article are the assessment of the impact of varying spatial and temporal integration lengths on these parameters, their dependencies on the integration volumes and area sizes, and the model for both temporal and spatial correlation parameters.

Index Terms— Fitting, modeling, radio-wave propagation, rain characteristics, rainfall rate, statistical model.

I. Introduction

RAIN-INDUCED attenuation of microwave signals at frequencies above 10 GHz is the dominant dynamic impairment on high-capacity satellite and terrestrial links [1], [2]. The parameters that are used to characterize rain at different spatial (L) and temporal (T) integration lengths is important as all the rain in the first Fresnel zone of a radio link leads to attenuation [3]–[6]. Network planners and designers of physical layer fade mitigation techniques [7], [8] require knowledge of rain characteristics at smaller space (L') and time (T') scales than are typically available from radar or rain gauge measurements. This provides impetus for the development of rain models which can be used to predict rain rates at fine scales.

Rain measurements produced by rain gauge, rain radar, and satellite, each have strengths and drawbacks [9], [10], [12].

Numerical models can be used to address their limitations and integrate their strengths appropriately [13], [14]. For example, Maseng and Bakken [15] proposed a stochastic-dynamic time-series model for rain attenuation field simulation, which was later extended to two locations in [16]. A study in [17] shows that Maseng's model also applies to rainfall rates with the same dynamic parameters. A space–time rainfall process model that describes the behavior of the stochastic structure of rain fields was proposed by Cam [18]. Many models have subsequently been proposed, i.e., [19]–[23], and many assume that rainfall intensity exhibits a lognormal distribution [24].

An understanding of rainfall behavior in both space and time at multi-resolutions is important for the development of rain attenuation models [4]. The study in [25] investigated the rainfall variability in Italy at different time scales from 30 to 720 min using both rain gauge and weather radar data. However, this study was limited to the spatial and temporal correlation functions of rain rate at different temporal scales. Luini and Capsoni [6] investigated the effect of space or time integration on the spatial correlation functions of rain separately but not combined. Understanding the effect of combined space–time integration on spatial correlation is important for the development of effective fade mitigation techniques and the space–time rain field simulators. Yang *et al.* [3] highlighted the importance of space–time averaging on rain properties.

This article focuses on the comprehensive study and modeling of the key rain properties over different spatial and temporal integration lengths (ranging from 5 to 75 km in space and from 15 to 1440 min in time) to investigate how scaling affects the dynamic–statistical properties of rain fields over different oceanic regions in North-Western Europe. The main aim is to ameliorate the challenges and cost of obtaining high-resolution rainfall rate characteristics over wide areas. It proposes models that can be used to obtain rain characteristics at multiple space (λL) and time (φT) scales. This article 1) characterizes rainfall fields over different climatic zones in North-Western Europe based on radar measurements. As rain is irregular in both space and time domains, its key characteristics with varying space–time scales at different locations are studied and presented and 2) proposes a new space–time statistical rain model for spatial correlation and temporal variation of rain over the whole of North-Western Europe. The results of higher-order moments of rain fields and empirical models of rain/no rain statistics are presented.

The rest of this article is organized as follows. Section II reviews space–time rain model implemented in this study. Details of the experimental data used are also provided. The methodology used to vary the integration length of radar data in both the space and time domains is presented in Section III. Section IV describes how to characterize the rain properties and the technique used to integrate the data from short to long integration lengths. Section V presents the results of rain rate statistics, spatial and temporal correlations of rain, the probability of rain/no rain, and the proposed empirical models. Conclusion is drawn in Section VI.

II. SPACE–TIME MODELING OF RAINFALL RATE

Rainfall rate, R, in mm/h, at a particular location and for a particular combination of spatial and temporal integration is modeled as a lognormal process with mixed probability density function (pdf) [1]

$$\Lambda_R(\mu, \sigma, P_0) = \begin{cases} 1 - P_0, & \text{no rain} \\ \dfrac{P_0}{\sqrt{2\pi}\,R\sigma} exp\left[-\left(\dfrac{ln R - \mu}{\sigma} \right)^2 \right], & \text{for rain} \end{cases}$$

$$(1)$$

where P_0 denotes the probability of rain occurrence ($R > 0$) and $\{\mu, \sigma\}$ are the lognormal parameters describing the average annual distribution of rainfall rate. The statistical parameters $\{P_0, \mu, \sigma\}$ depend on the location $\mathbf{x} = (x_1, x_2)$ and the spatial and temporal integration lengths. Crane [1] has shown that the spatial correlation function of rain rate depends only on the separation distance between two locations and the 2-D spatial correlation function can be assumed to be isotropic, i.e., it takes the form $c_S(x, y) \equiv E[R(\mathbf{x}, t_1)R(\mathbf{y}, t_1)] \equiv c_S(d)$, where $d = |\mathbf{x} - \mathbf{y}|$. The temporal correlation function between rainfall rate at the same location but separated by a duration of $\tau = |t_2 - t_1|$ can be represented by $c_T(t_1, t_2) \equiv E[R(\mathbf{x}, t_1)R(\mathbf{y}, t_2)] \equiv c_T(\tau)$.

The assumptions of stationarity and homogeneity greatly reduce the complexity of rain field characterization. The point statistics (including rain/no rain) and the spatial and temporal correlation functions form a basic set of "key characteristics" from which rain fields can be numerically synthesized. Bell [24] showed how rain fields can be numerically synthesized. However, he assumed that all locations within a wide area share the same statistics. This is unrealistic for large area communication networks as rainfall rate varies from location to location, influenced by factors such as climate, topography, and wind. Although this problem has been solved by an approach proposed by Jeannin *et al.* [26], a detailed study on the rain characteristics is needed to understand the variability of rain, especially those at multiple space and time resolutions.

III. DATA DESCRIPTION

The rainfall rate data used in this study has been obtained from the U.K. Metrological Office NIMROD radar system in the form of composite spatial maps spanning oceanic climates in North-Western Europe produced at a temporal interval of 15 min and integrated over square regions of
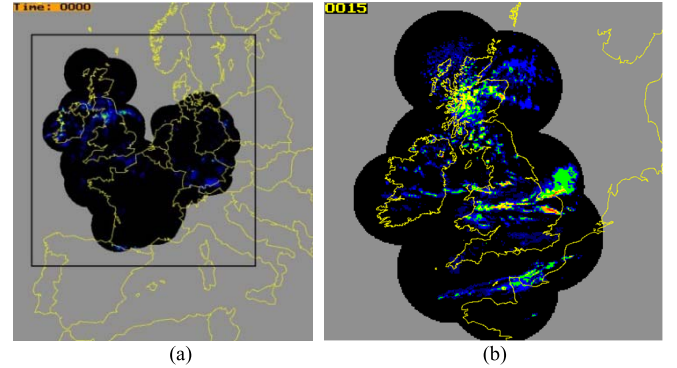

Fig. 1.   NIMROD composite images of precipitation rates for (a) Central North-Western Europe with a dimension of 2000 km × 2000 km and 5 km resolution and (b) British Isles with 1 km sampling.

dimension 5 km × 5 km. The NIMROD data are available from the British Atmospheric Data Centre (BADC), one of the Natural Environment Research Council (NERC) centers for atmospheric sciences. The NIMROD data are continuously updated and the BADC ensures the long-term integrity of the data. Over the U.K., NIMROD also provides data on a 1 km grid acquired with a sample time resolution of 5 min but with variable spatial resolution depending on the distance to the nearest radar. The NIMROD data have been validated using rain gauge data by some researchers, i.e., [27], and a range of data is used to calibrate the radars. Some differences between the NIMROD and rain gauge data are expected due to spatial averaging. The NIMROD 1 km data have been shown to yield unbiased estimates of annual 0.01% exceeded rain rates [28].

The NIMROD network consists of 15 C-band weather radars that cover the whole British Isles. They scan at high space and time resolutions over long distances. Four to five radars repeat the scan at different elevations to build 3-D scans of the area from which the best estimates of rain rates on the ground are established (details about the NIMROD radar system are given in [27]). A series of composite rain field maps are then produced of rainfall rate samples on a 5 km squared Cartesian grid covering North-Western Europe. Each map contains 700 × 620 data cells. However, in this study, a 400 × 400 grid, i.e., a 2000 km square region, in each radar image has been analyzed. This spans the irregular shape covered by the radars. The study area ranges from 43.1938° to 59.4306° in latitude and −9.7370° to 19.8364° in longitude. Five years of composite rain radar maps (2005–2009) have been analyzed in this study. The full data set consists of more than 166 000 radar maps with data availability of over 90% for each year. Fig. 1(a) shows a typical NIMROD radar scan image. The gray color is the area outside the range of the radar network where no rain data are available, and the black color represents the scanned area where data are available. A typical composite rain rate image of the U.K. is shown in Fig. 1(b). The validation of a model's performance requires comparisons of estimates to be made with measured data (e.g., from rain gauge or rain radar) [10]. Therefore, the 1 km grid U.K. data can be used to validate the results of an interpolation approach that is applied to the 5 km grid radar data for the U.K.

The NIMROD system uses data collected from range height indicator scans at several elevations to estimate the

Location	Glasgow	Paris	Portsmouth	Rennes	Reims
Latitude	55.8642	48.8566	50.8198	48.1173	49.2566
Longitude	-4.2518	2.3522	- 1.0879	-1.6778	4.0331

rain rates at different altitudes and combines these data sets to predict the rain rate at ground level. Due to the complex spatial–temporal processing involved, the ground rain rates are not quantized. The processing is described in [29]. The NIMROD radar provides rain-rate estimates over a large area but the resolution is not high enough for applications in radio propagation. In particular, the design and planning of the next-generation satellite networks requires knowledge of rain variation over much shorter scales, i.e., a typical Fresnel zone of a few tens of meters. The NIMROD data, which are generated every 15 min on 5 km Cartesian grid, do not meet this requirement, and, hence, the work reported in this article.

Rain characteristics at many locations within Western Europe have been studied to reveal the impact of scaling and space–time averaging on the dynamic–statistical properties of rain fields. The latitudes and longitudes of five studied locations are listed in Table I.

IV. CHARACTERIZATION OF RAINFALL FIELDS

A. Rainfall Rate

The composite map is represented on a Cartesian grid and each point contains space–time-averaged rain intensity information. The average rainfall rate centered on the origin over time T and spatial area $A = L^2$ can be expressed as in [4]

$$R(L, T) = \frac{1}{T} \int_{-T/2}^{T/2} dt \frac{1}{L^2} \int_{-L/2}^{L/2} \int_{-L/2}^{L/2} r(\boldsymbol{x}, t) da \quad (2)$$

where $r(\boldsymbol{x}, t)$ denotes the point rainfall rate in mm/h at location $\boldsymbol{x}$ and time t on a 2-D Cartesian grid. The interval T is the temporal integration length, while L is the spatial integration length. Each NIMROD radar map consists of a Cartesian grid of such space–time-averaged values. Each value is an estimate of rainfall rate at a particular instant but the algorithm for deriving the rain rate yields a value consistent with a particular integration period.

B. Key Characteristics of Rain

Four key rain parameters are needed to develop a space–time rain attenuation field model [3]. The principal parameter is the annual probability distribution of rain. Many studies have shown that point rainfall rate is well modeled as a log-normal random variable with a pdf given by

$$f(R) = \frac{1}{\sqrt{2\pi} R \sigma} exp\left(-\frac{1}{2}\left(\frac{ln R - \mu}{\sigma}\right)^2\right) \quad (3)$$

where μ and σ are the mean and standard deviation of log rainfall rate, respectively. It is possible to transform the complementary cumulative distribution function (CCDF) to a linear relationship as described in [30]. The application

of this statistical technique to different spatial and temporal integration lengths is discussed in Section V. Estimating μ and σ requires a tradeoff between acquiring a large enough sample to yield significant estimates and remaining within a homogenous climate region of rain regime.

The spatial correlation function is the second important characteristic and is expressed as follows:

$$\rho = \frac{cov(R_1, R_2)}{\sqrt{\sigma_1 \sigma_2}} \quad (4)$$

where R_1 and R_2 are the rainfall rates (mm/hr) at two locations 1 and 2, respectively, ρ is the cross-correlation factor between R_1 and R_2, and $cov(*)$ and σ are the covariance and standard deviation, respectively. In [3] and [22], it is assumed that the spatial correlation function of rainfall rate only depends on the separation distance, i.e., the rain rate fields are spatially homogeneous, isotropic, and stationary in time. These assumptions are mainly valid over small distances and times such that the shape of rain field and intermittence of rain events have no effect. Rain fronts and squalls have large linear features which are not homogeneous or isotropic over event scales. Theoretically, the correlation in space will be the same in any horizontal direction and, therefore, can be computed using pairs of rain rates in any orientation.

Typically, intense rain showers, which cause extreme attenuation, are of short durations. Temporal correlation quantifies how rain intensity at one particular location is correlated over different times. Temporal correlation is important as it is linked to temporal variation of fade, especially for high elevation links, which is a major input in the design of fade mitigation schemes. The development of effective route diversity or site diversity networks requires detailed knowledge of both the temporal and spatial correlation functions of rainfall rate. The temporal correlation function is defined by

$$\rho = \frac{cov(R_{t_1}, R_{t_2})}{\sqrt{\sigma_1 \sigma_2}} \quad (5)$$

where R_{t_1} and R_{t_2} are the point rainfall rates (mm/h) at two different times t_1 and t_2 but at the same location.

The last important parameter considered in this study is the probability of rain occurrence (P_0) in a geographical area, which is chosen to be of a similar size as the spot beam of a satellite network [22]. Theoretically, P_0 (for which $R > 0$) represents equally well the expected fraction of the rainy area that one can expect for a satellite or the probability of rain occurrence at one point over a period of time [3]. If an unbiased sample of rain maps is available for a homogeneous climate area, then the parameter P_0 may be estimated using

$$P_0 \cong \frac{1}{M} \sum_1^M \frac{A_{rainy}}{A_T} \cong \frac{1}{N_T} \sum_1^{N_T} \frac{N_{rainy}}{N} \quad (6)$$

where A_{rainy} is the area experiencing rain within a map, A_T is the total area of the rain map of interest, M is the number of maps, N_{rainy} is the rainy sample amount at one grid point, N_T represents the total samples (including rain and no rain) at that point over a long period, and N is the total number of grid points in the area A_T.

C. Integrated Rainfall Data

Radar-derived space–time rainfall data typically span a larger area than rain gauge networks [10] and provides considerably denser spatial sampling. A rainfall rate map may be used to simulate the instantaneous joint fade experienced by all the links in an arbitrary microwave network [31], [32]. However, the problem lies in the reduced quality originating from the coarse sampling of measured maps as this is linked to the scan rate of the radar.

One of the key objectives of this article is the assessment of the impact of varying spatial integration lengths and temporal integration lengths on the studied quantities. This will be useful to enhance the ability to predict the rain-induced attenuation at a range of spatial–temporal resolutions.

Let $R(x, y, t)$ be the measured rainfall rate with space resolution L and time resolution T. $R(x, y, t) = R_{ijk}$ if $iL \leq x \leq (i + 1)L$, $jL \leq y \leq (j + 1)L$, and $iT \leq t \leq (k + 1)T$, otherwise $R(x, y, t) = 0$. This definition yields a 3-D array of measured rain rate values with spatial averaging regions of size $L \times L$ and a sampling interval of T. Consider the 3-D indicator function

$$I(x, y, t) \equiv \begin{cases} 1 & |(x, y, t)|_\infty < \frac{1}{2} \\ 0 & otherwise \end{cases} \quad (7)$$

can be used to define how the rainfall rate changes with integration volume, where $|(x, y, t)|_\infty$ is the infinite norm. The multi-scale rainfall rate fields are defined as

$$R_\lambda(x, y, t) = \frac{1}{\lambda^3 L^2 T} \int \int \int R(x', y', t') I$$
$$\times \left(\frac{x - x'}{\lambda L}, \frac{y - y'}{\lambda L}, \frac{t - t'}{\lambda T} \right) dx' dy' dt' \quad (8)$$

where $R_\lambda(x, y, t)$ is the rainfall rate at position (x, y) derived from a spatial integration region of linear size λL and temporal integration time λT, where $\lambda > 1$ is known as the scale parameter. More generally, the spatial and temporal regions could have different scale parameters, e.g.,

$$R_\lambda(x, y, t) = \frac{1}{\lambda^2 \varphi L^2 T} \int \int \int R(x', y', t') I$$
$$\times \left(\frac{x - x'}{\lambda L}, \frac{y - y'}{\lambda L}, \frac{t - t'}{\varphi T} \right) dx' dy' dt'. \quad (9)$$

In particular, the integration can be divided into three categories: 2-D spatial integration, 1-D temporal integration, and 3-D spatial–temporal integration. The 2-D spatial integration only changes the integration length in the space domain at a fixed time and the 1-D temporal integration is at a fixed location. The 3-D integration is particularly interesting as the rain event evolves in both space and time simultaneously. It is, therefore, a combination of both spatial and temporal integration.

V. EXPERIMENTAL RESULTS AND ANALYSIS

A. Statistics of Rain

1) Experimental Results: Generally, rain measurements are carried out at uniform time intervals. For a particular location, the annual CCDF of point, 1 min rain intensities can
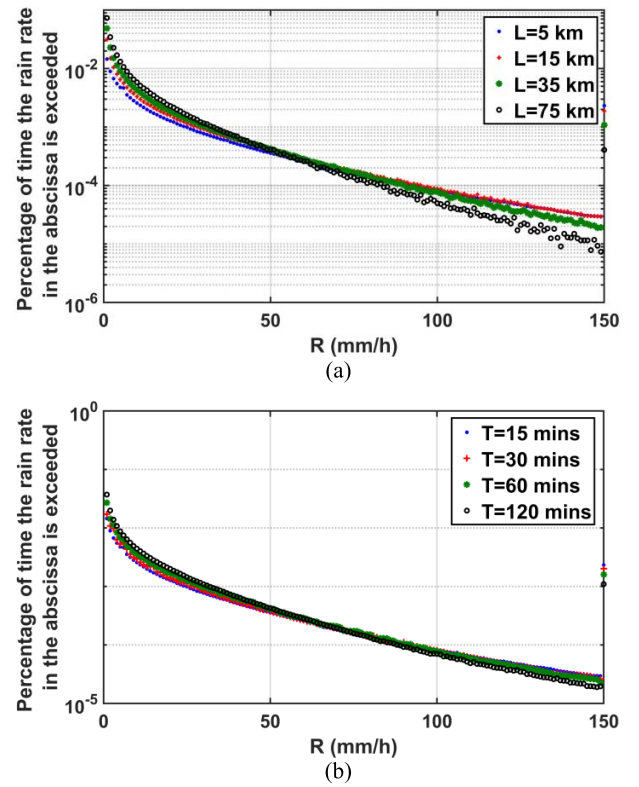

Fig. 2. Averaged CCDF of 5 year NIMROD rainfall rate data for a range of integration lengths. (a) Space domain with a time interval of 15 min. (b) Time domain with a space resolution of 5 km.

be generated. In this article, Portsmouth (U.K.) is taken as an example to discuss the results in detail. Fig. 2 shows the CCDF of rainfall rate conditioned on the occurrence of rain for the rainfall rate above 1 mm/h. It shows that the probability of a spatial–temporal volume containing rain gradually increases with the increasing integration length in both the space and time domains, respectively, up to around 60 mm/h in space and 65 mm/h in time.

Using the technique described in [30], the CCDF can be transformed to test its log-normality. A normal distribution leads to a straight line given by

$$Q_{inv} = \frac{ln(R)}{\sigma} - \frac{\mu}{\sigma} \quad (10)$$

where μ and σ are the log-normal mean and standard deviation, respectively, and Q_{inv} is the inverse function of CCDF.

Fig. 3 shows the data and least squares (LSQ) linear regression fit to the log-normally transformed data for spatial integration lengths from $L = 5$ km to $L = 75$ km ($T = 15$ min) and temporal integration lengths from $T = 15$ min to $T = 120$ min ($L = 5$ km). These results support the hypothesis that rainfall rate distributions can be well approximated by log-normal distributions. However, note the systematic deviation for rain rates with $In(R) > 3$ for all spatial integration lengths. This is consistent with the findings in [33].

Tables II and III list all the estimated parameter values (μ and σ) for Portsmouth for different spatial and temporal integration lengths. The value of μ gradually increases with increasing integration length, meanwhile for the value of σ, the
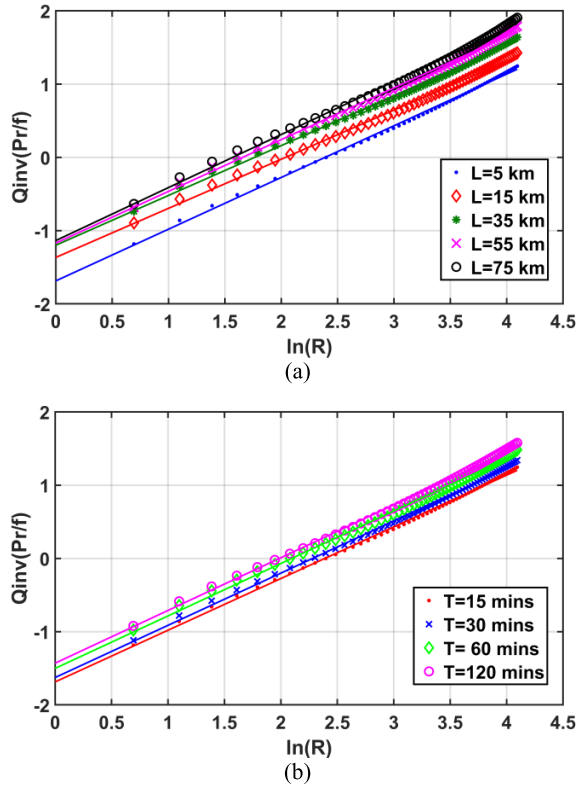
Fig. 3. Test for log-normality of rainfall rate distribution for different integration lengths. (a) Space domain with a time interval of 15 min. (b) Time domain with a space resolution of 5 km.

TABLE II

EXPERIMENTAL COEFFICIENTS VALUE OF LOG-NORMAL DISTRIBUTION PARAMETERS FOR DIFFERENT SPATIAL INTEGRATION LENGTHS AT PORTSMOUTH ($T = 15$ min)

L (km)	5	10	15	20	25	35
μ	−3.35	−3.21	−3.00	−2.97	−2.79	−2.67
σ	1.99	1.84	1.71	1.66	1.59	1.52
L (km)	40	45	50	55	65	75
μ	−2.60	−2.52	−2.45	−2.41	−2.33	−2.28
σ	1.48	1.49	1.43	1.39	1.31	1.22

TABLE III

EXPERIMENTAL COEFFICIENTS VALUE OF LOG-NORMAL DISTRIBUTION PARAMETERS FOR DIFFERENT TEMPORAL INTEGRATION LENGTHS AT PORTSMOUTH ($L = 5$ km)

T (min)	15	30	45	60	75	90	105	120
μ	−3.35	−3.16	−3.00	−2.95	−2.82	−2.78	−2.77	−2.64
σ	1.99	1.81	1.72	1.67	1.60	1.56	1.49	1.43

coarser the resolution, the smaller it becomes. The consistency of these changes has been tested using 1 km spatial grid U.K. NIMROD data.

Fig. 4 gives values of μ and σ for different map sizes, S, from 5 km $\times$ 5 km to 530 km $\times$ 530 km, with $L = 5$ km and $T = 15$ min. It shows that both μ and σ values significantly change for small areas $S < 200$ km $\times$ 200 km. These values gradually become stable and converge to constant values when the size of the map is greater than 400 km $\times$ 400 km.
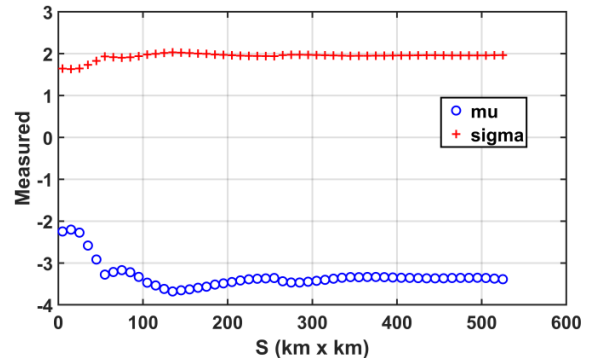

Fig. 4. Experimental values of parameters of fitted lines for different map sizes **S** centered at Portsmouth with $L = 5$ km and $T = 15$ min.

This happens for all spatial and temporal integration lengths (all figures are not presented in this article). Apparently, this indicates that when studying the rain field structure over a large area where there is no strong orographic effect and for which the climate is relatively homogeneous, the statistics of rain is independent of the map size and the integration volume is the factor that needs to be considered.

2) Validation: The Chi-squared test was applied to evaluate how well the observed trend can be used to predict rainfall at different space and time resolutions. Fig. 5(a) shows the comparison between equal-probability bin histograms of rainfall rates observed and fitted ($L = 5$ km and $T = 15$ min). Fig. 5(b) shows the predicted results in comparison with the measured data based on the proposed technique. Given that rainfall rates above 30 mm/h is important for satellite communications, the results in Fig. 5(b) show that the probability of rain is between 0.01% and 0.001%. The dotted line is the 5 year average from the measured data, while the solid line is the best fit of the model. The fitted curve appears plausible up to 35 mm/h, after which divergence occurs. However, it should be noted that the probability of exceedance at these higher rainfall rates are based on a small number of samples.

Fig. 6 shows the rainfall rate exceeded for 0.01% in an average year given by Rec. ITU-R P. 837-7 [34] using 1 min temporal integration length of rainfall rate. This is useful for the prediction of rain attenuation in radio communications. The rainfall rate is in the range 30–60 mm/h in Western Europe. In the Portsmouth area, the rainfall rate exceeded for 0.01% of time is approximately 30 mm/h, which is larger than the 5 km instantaneous 0.01% rainfall rate exceeded as shown in Fig. 5(b).

Comparing rain model predictions with measured data is commonly performed to validate the model's performance. However, the model proposed in this article does not predict the rainfall rate directly but the derived key characteristics of rain. Because of this, it is necessary to compute the parameters from measured data and compare them with the proposed model predicted rain characteristic parameters to validate the model's performance. The NIMROD database holds two data sets provided by different agencies: one data set is for North-Western Europe and the radar stations are located in North Europe and are operated by European agencies and the other is for the British Isle and the data set
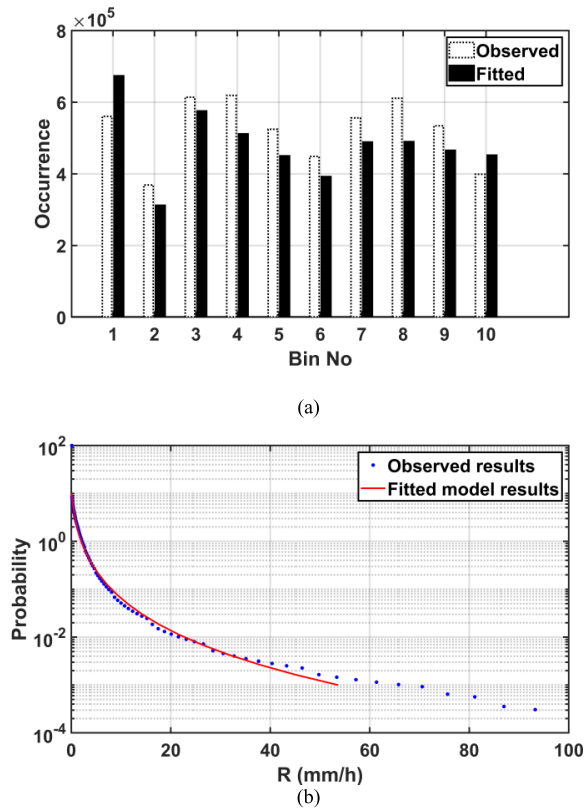
(a)

(b)

Fig. 5.   Comparison between the observed and fitted results. (a) Near-equal probability histograms of rainfall rate. (b) Rainfall rates exceedance distribution, here $L = 5$ km and $T = 15$ min.

is provided by the U.K. Met Office for radar stations located in the U.K. The advantage of the North-Western Europe data set is its large coverage, but the resolution is 5 km in space and 15 min in time. This data set has been extensively used in this article to develop the model. The data set for the British Isle provided by the U.K. Met Office only covers the British territory but offers better resolutions (1 km in space and 5 min in time). Because the radar stations that generate these two data sets estimate the rain rate at different azimuth scans, times, and elevations, the upscaling of 1 km U.K. NIMROD data to 5 km will be different from the North-Western Europe data for the British Isle. However, the key characteristics of rain parameters would be expected to be similar. This has enabled the proposed model to be developed using on set and the other data set to be used for validation.

The U.K. NIMROD data (1 km sampling in space and 5 min in time) have been integrated to form 5 km × 5 km grids to approximate the EU NIMROD data. Fig. 7 compares the rainfall rate exceedance distributions at Portsmouth (U.K.) from radar-derived EU NIMROD data and the U.K. data (the average over 5 years). It shows that after the integration, the rainfall rate exceedance distribution generated from the different databases are in strong agreement. The fitted curve to the U.K. NIMROD data is slightly lower than the fitted curve to the EU NIMROD data. The observed rainfall rates exceeded for 0.1%, 0.01%, and 0.001% of the time from both EU and U.K. data at Portsmouth are {7.85 mm/h, 23.9 mm/h, 67.9 mm/h} and {7.6 mm/h, 21.7 mm/h, 66.3 mm/h}, respectively.
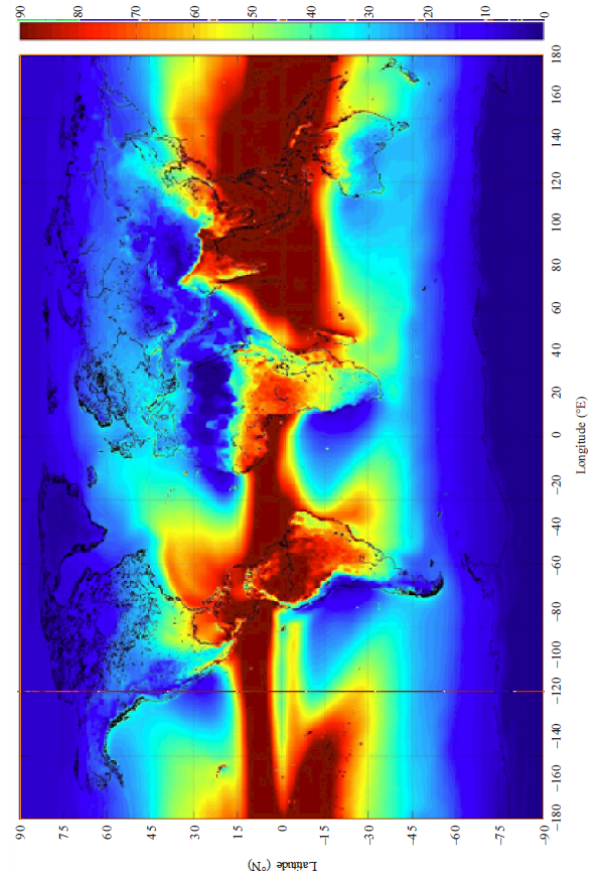

Fig. 6.   Rainfall rate (mm/h) exceeded for 0.01% of the average year given by Rec. ITU-R P. 837-7.
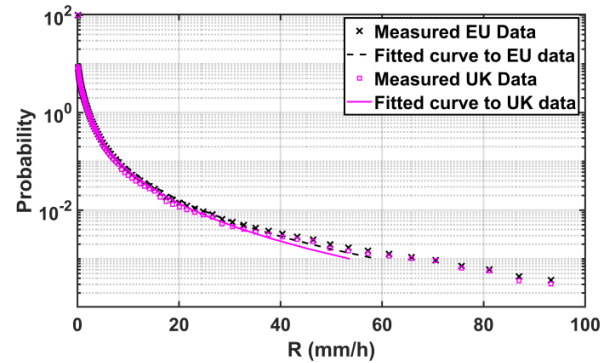

Fig. 7.   Comparison of rainfall rate exceedance distribution at Portsmouth using the EU and U.K. data averaged over 5 years.

B. Correlation Function of Rain

Spatial and temporal correlation functions of rainfall rate are important for rainfall field modeling and simulation [35], [36]. They vary depending on location, climate, topography, rainfall type, etc. [37]–[39]. The impact of space and time averaging on the autocorrelation function is of particular interest [3]. All these factors should be taken into account in the prediction of rain-induced attenuation.

1) Spatial Correlation Function of Rainfall Rate: The horizontal structure of rainfall fields, hence spatial correlation
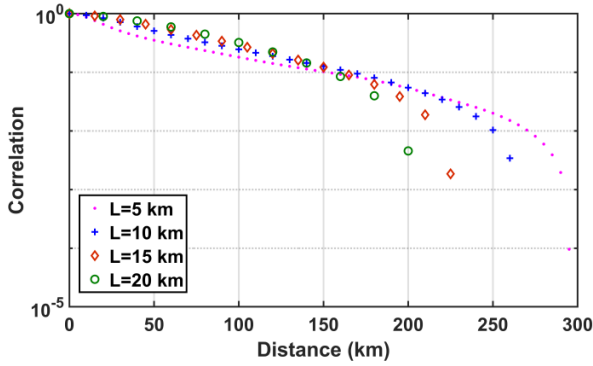
Fig. 8. Spatial correlation function of rainfall rate for different spatial integration diameters at Portsmouth (here $T = 15$ min).

Fig. 9. Example of fitted spatial correlation function of rainfall rate with $L = 5$ km and $T = 15$ min.

between two points, is important for high-frequency wireless network planning [40]. Many empirical models have been proposed and each model is derived from a study of different regions covering different continents and for rainfall rate measurements with a range of integration volumes. The differences among these models indicate that the spatial structure of rainfall fields strongly depends on climate, topography, etc. Manabe *et al.* [41] argued that an exponential distribution is more suitable for European regions and can be adapted to other areas. Other exponential models have been proposed in [35], [42]–[44].

This study has produced a general empirical equation that fits both the spatial and temporal correlation functions of rain rate. The generalized model is given by

$$\rho = \frac{a}{a + x^q} \qquad (11)$$

where $a > 0$ and $q > 0$ are parameters to be determined, and x can either be d (where d represents the distance in kilometers) or t (where t is the time lag in minutes).

In this study, 5 years of rainfall rate data have been analyzed to estimate the spatial and temporal correlation functions of rainfall rate. Fig. 8 shows the spatial correlation function of rainfall rate at Portsmouth for different spatial integration lengths ranging from $L = 5$ km to $L = 20$ km. It shows that spatial correlation increases with increasing integration length due to the mixing of point covariance, with the larger covariance dominating. For example, let $C(z) = E[R(x)R(x + z)]$ be the second moment of the point rainfall rate process. For rain integrated over a line $R_D(x) = (1/2d) \times \int_{x-d}^{x+d} R(z)dz$, where d is distance, the second moment is

$$R_D(x) = E[R_D(x)R_D(x + z)]$$
$$= \frac{1}{(2d)^2} \times \int_{x-d}^{x+d} \int_{x+z-d}^{x+z+d} E[R(z_1) * R(z_2)]dz_1 dz_2.$$

As long as $C(z)$ is decreasing and convex then $C_D(z) > C(z)$. The nearlinear sections of the curves (see Fig. 8) suggest exponential correlations. In particular, the 5 km data suggest that there are two exponential regions: from 0 to 50 km and 50 to 200 km. This is less obvious for larger integration length due to the effect of averaging. Fig. 9 illustrates the performance of the proposed correlation
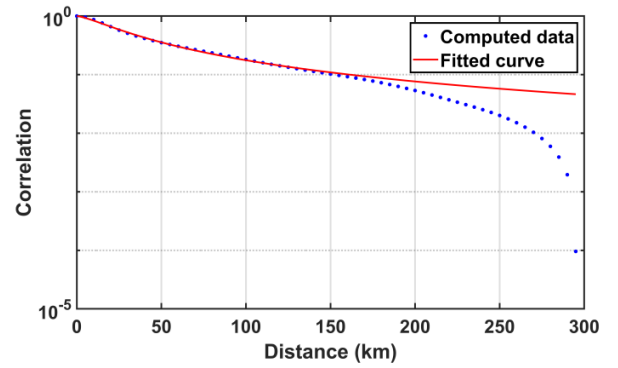
TABLE IV
EXPERIMENTAL PARAMETER VALUES OF SPATIAL CORRELATION
FUNCTIONS OF RAINFALL RATE FOR EACH SPATIAL
INTEGRATION LENGTH AT PORTSMOUTH ($T = 15$ min)

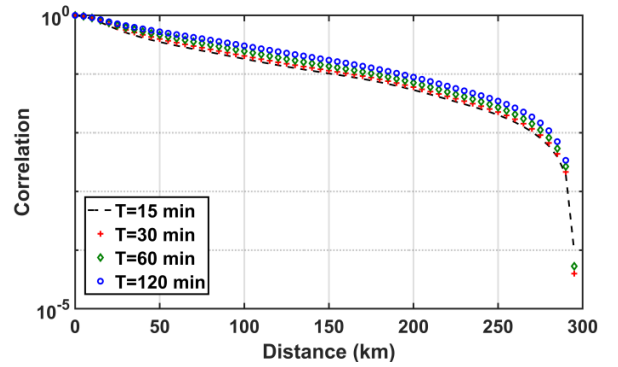| L (km)	5	10	15	20
a	118	494	615	884
q	1.37	1.58	1.74	1.81

Fig. 10. Spatial correlation function of rainfall rate for different temporal integration lengths at Portsmouth (here $L = 5$ km).

function model [see (11)] against values from measured data at 5 km in space and 15 min in time resolutions. This shows that the correlation values can accurately be predicted using the proposed model for distances up to 150 km. The fitting has been accomplished by the minimization of the error function

$$Error = \sum |Corr_{fitted} - Corr_{measured}| \qquad (12)$$

where $Corr_{fitted}$ is the fitted correlation function and $Corr_{measured}$ is the measured value.

Note that the correlation curve rapidly falls off beyond 150 km. There is no suitable model for distances above 200 km, even the published models. Table IV lists the model parameter values obtained from fitting the proposed model for different spatial integration lengths from 5 to 20 km.

Fig. 10 shows the computed spatial correlation function of rainfall rate with different temporal averaging. The EU NIMROD data provide near-instantaneous rainfall rates at 15 min sampling intervals. Averaging n consecutive rainfall rate values for the same 5 km diameter region yields a coarse

TABLE V

EXPERIMENTAL PARAMETER VALUES OF SPATIAL CORRELATION FUNCTIONS OF RAINFALL RATE FOR EACH TEMPORAL INTEGRATION LENGTH AT PORTSMOUTH ($L = 5$ km)

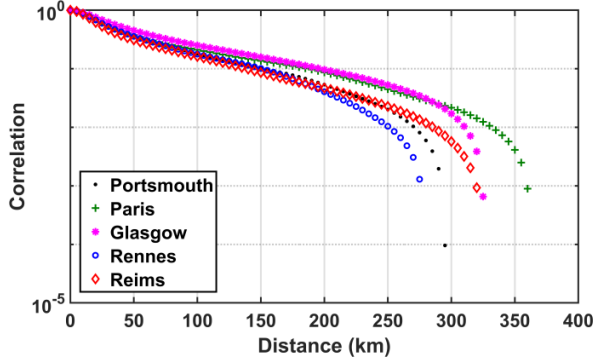| T (min)	15	30	45	60	75	90	105	120
a	117	165	206	221	222	205	218	214
q	1.37	1.41	1.43	1.42	1.40	1.37	1.36	1.35

Fig. 11. Comparison of spatial correlation functions of rain, for five European locations, derived from 5 years of radar data (here $L = 5$ km and $T = 15$ min).

estimate of the $(n-1) \times 15$ min temporal integration. It shows that temporal correlation also increases with increasing temporal integration length, similar to spatial correlation. The fitted parameter values for integration lengths from 15 to 120 min are given in Table V.

Five locations distributed across the Western European radar-scanned area were investigated to assess how spatial and temporal correlation functions of rainfall rate change with location. Fig. 11 presents their spatial correlation functions calculated using 5 years of data. The spatial correlation is very close for all locations for the scales (0−15 km), which is a typical scale for rain storms. For larger scales, the spatial correlation is more variable with increasing differences between the locations. This is consistent with the findings of Manabe *et al.* [41] who studied eight locations in Europe. The large difference in correlation values between Paris and Rennes suggests a strong climatological or topographic dependency. It also shows that all the distributions are close to exponential over the range 50 200 km. The range beyond 300 km yields negative correlation values. This could be used to optimize diversity gain when choosing locations for satellite ground stations. For all locations studied, the proposed correlation model [see (11)] provides a very good fit to the calculated values. This supports the results reported in [40]. In addition, the authors have relied on the NIMROD system to produce the unbiased results. Although the resolution of the data will be higher nearer radars, this should not affect the correlation. The rain fields have been assumed to be isotropic and, hence, the correlations to be rotationally symmetric. It seems more reasonable to assume that maritime and continental locations will experience a different mix of weather systems and so exhibit different correlation functions.

2) Temporal Correlation Function of Rain Rate: The temporal correlation function of rainfall rate is important for
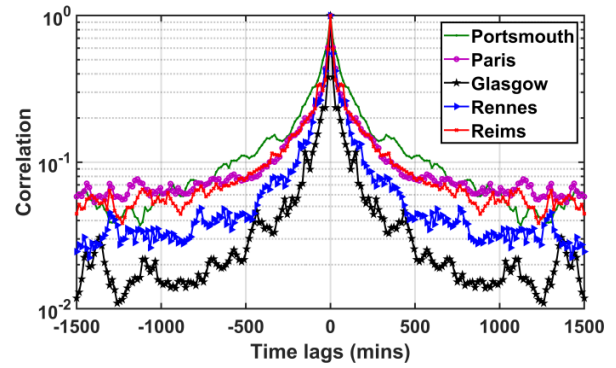

Fig. 12. Temporal correlation function of rainfall rate for five European locations, here $L = 5$ km and $T = 15$ min.
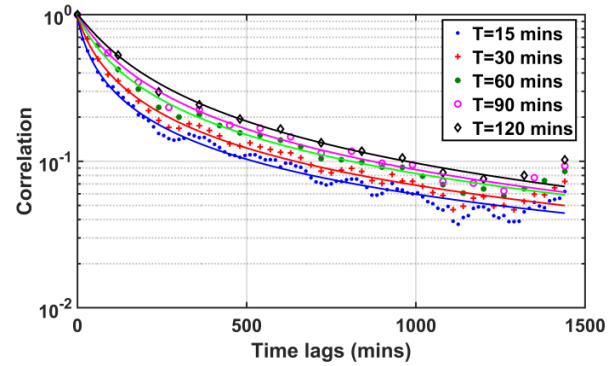

Fig. 13. Fitted lines for the temporal correlation function of rainfall rate with different temporal integration lengths at Portsmouth, here $L = 5$ km.

TABLE VI

EXPERIMENTAL PARAMETER VALUES OF TEMPORAL CORRELATION FUNCTION OF RAINFALL RATE FOR DIFFERENT TEMPORAL INTEGRATION LENGTHS AT PORTSMOUTH ($L = 5$ km)

T (min)	15	30	45	60	75	90	105	120
a	24.1	45.5	60.6	84	102	136	193	215
q	0.86	0.93	0.96	0.99	1.01	1.05	1.09	1.10

network reliability design, sufficient link power margin provision, and adequate fade mitigation employment. Fig. 12 compares the temporal correlation functions of rainfall rate of the five European locations based on 5 year data. At a correlation value of 0.37 (equal to the value of $1/e$), correlation times of between 60 and 200 min are obtained at different locations indicating a strong location dependency. Fig. 12 also shows that the temporal correlation function of rainfall rate significantly changes with temporal integration lengths between 15 and 120 min. Similar results have been reported in [45] for sampling periods of 10 s and 1 min using data measured using a disdrometer.

The data and the fitted curves based on (11) for different temporal integration lengths are provided in Fig. 13. The fitted curves are in good agreement with the measured data for time lags up to 1000 min. The values of the parameters of (11) for each temporal integration length are provided in Table VI.

Fig. 14 shows the short-lag temporal correlation function at Portsmouth for different spatial integration lengths ranging from $L = 5$ km up to $L = 75$ km with $T = 15$ min.
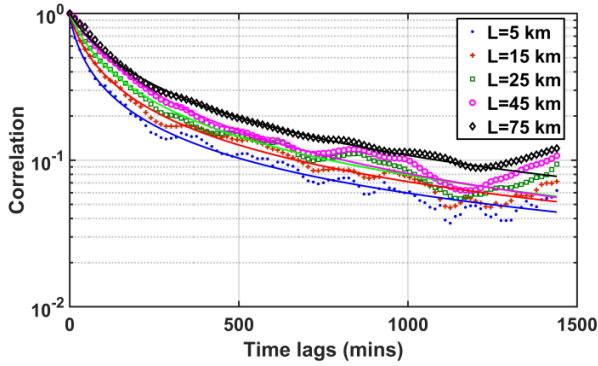
Fig. 14. Temporal correlation function of rainfall rate for different spatial integration lengths at Portsmouth, here $T = 15$ min.

TABLE VII

FITTED PARAMETER VALUES OF TEMPORAL CORRELATION FUNCTIONS OF RAINFALL RATE FOR EACH SPATIAL INTEGRATION LENGTH AT PORTSMOUTH ($T = 15$ min)

L	5 km	10 km	15 km	20 km	25 km	35 km
a	24.1	24.6	44.2	59.9	74.8	87.4
q	0.86	0.87	0.92	0.96	0.98	0.99

L	40 km	45 km	50 km	55 km	65 km	75 km
a	141	176	211	266	331	383
q	1.07	1.10	1.04	1.22	1.24	1.00

It shows that the temporal correlation function gradually becomes smoother due to spatial averaging with increasing integration length.

The differences between the temporal correlation between $L = 5$ km and $L = 75$ km indicate a strong integration length dependency. However, the temporal correlation quickly falls off for any spatial integration length with short time lags to below 0.37 (roughly $1/e$) at approximately 500 min. The fitted parameter values of the proposed mathematical model are given in Table VII.

Typically, the temporal correlation function of point rainfall rate is affected by advection. The variation of rainfall rate at a point is due to two processes; the evolution of the rain event and the movement of the rain event. Rain event evolution tends to be slow but dominates at time lags of 40 min or longer, while the movement of rain event over a point dominates for short time lags. This variation is modeled as the movement (advection) of a fixed pattern of rain over a point using the frozen storm hypothesis [46]. It states that the statistics of rain at a point is the same as the statistics of rain along a line parallel with advection. The interpretation of this is $R(\mathbf{x}_0, t) = R(\mathbf{x}_0 - V(t - t_0), t_0)$, where V is the advection vector, and $\mathbf{x}_0$ and t_0 are an arbitrary position and time, respectively. This means that for time lags less than 40 min, the temporal covariance of point rainfall rate for a lag $\tau = (t - t_0)$ is the same as the spatial covariance for a spatial lag of $|V * \tau|$, assuming that the rain field is homogeneous and isotropic. The temporal correlation presented is the actual correlation experienced at a point. At short time lags, it averages over the range of advection speeds experienced. For lags greater than about 40 min, the results are determined
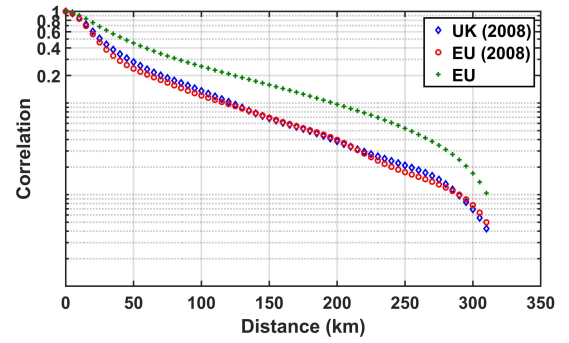

Fig. 15. Comparison of spatial correlation function of rainfall rate at Portsmouth achieved from different databases ($L = 5$ km and $T = 15$ min).

by a combination of the evolution of large rain events and the clustering of rain events.

3) Validation: Comparing rain model predictions with measured data is commonly performed to validate the model's performance. The predictions of the model proposed in this article, however, are not rainfall rates but the derived key characteristics of rain. Because of this, it is necessary to compute the parameters from measured data and compare them with model-predicted rain characteristics parameters to validate the model's performance.

One year of U.K. NIMROD data (2008) have been used to validate the model's performance. The data have been upscaled to achieve the same integration length as the EU data with 5 km spatial resolution and 15 min time resolution. Fig. 15 presents the spatial correlation function of rainfall rate at Portsmouth estimated from both the EU NIMROD database and U.K. NIMROD database. It compares the U.K. and EU data of 2008 and a combined 5 years (2005–2009) of the EU NIMROD data. The upscaled U.K. 1 km grid data from 2008 yield very similar results as the EU 5 km data for the same period. This provides assurances of the validity of the approach adopted. The curve derived from combining 5 years of EU data is significantly different showing that there could have been significant year-to-year rainfall rate variations. The two near-exponential ranges, from 0 to 50 km and between 50 and 200 km, are present in all curves. This suggests that the same processes are present but in different proportions. This finding is in accordance with the results presented in Figs. 8–11.

Fig. 16 compares temporal correlation functions of rainfall rate at Portsmouth using data from the EU NIMROD database and U.K. NIMROD database for 2008. Although there is a small difference, the results show that the proposed approach gives good estimates of data at one location.

C. Probability of Rain Occurrence

The probability of rain occurrence P_0 has been studied using 5 years of radar data. Each location has its own P_0 value and the P_0 value for any size of map can be obtained by averaging the P_0 values of all points within that map. It should be noted that the value of P_0 is poorly defined, as it is very difficult to tell whether rain is light or it is not raining at all. Its value is influenced by the way rainfall rate is measured as many instruments become unreliable at low rainfall rates. For radars,
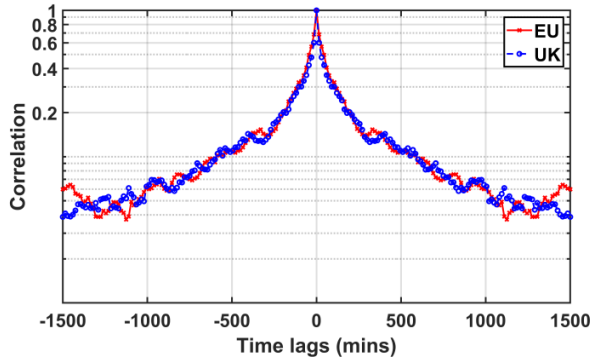
Fig. 16. Comparison of temporal correlation function of rainfall rate at Portsmouth achieved from both the EU NIMROD database and U.K. NIMROD database, for $L = 5$ km and $T = 15$ min.
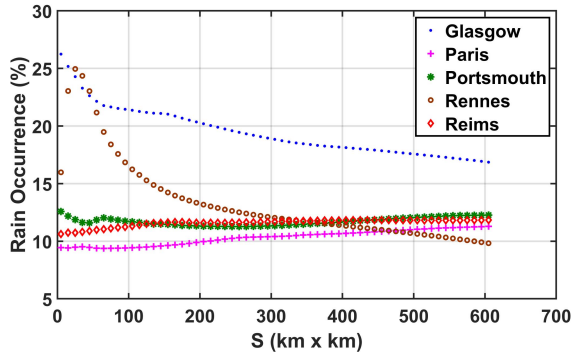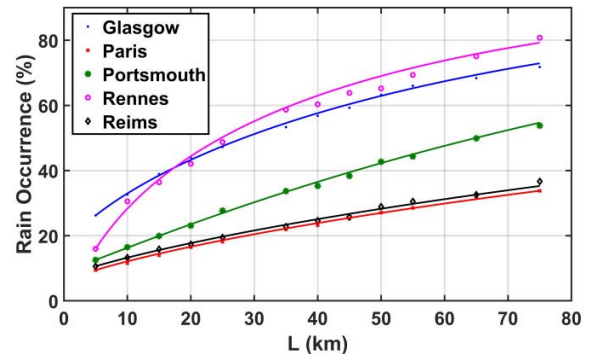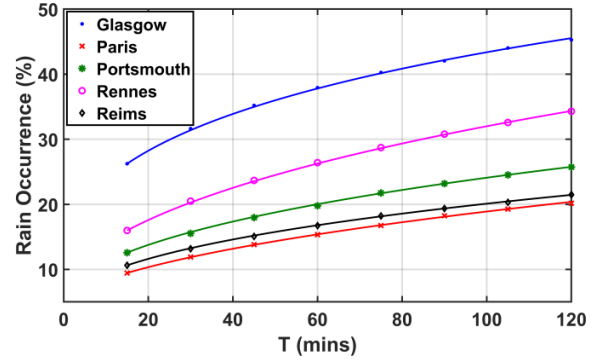

Fig. 17. Variation in probability of rain occurrence for five locations changes with an increasing size of map, here $L = 5$ km and $T = 15$ min.

Fig. 18. Probability of rain occurrence for increasing integration length in Europe. (a) P_0 for different spatial integration lengths L(km) and (b) P_0 for varying temporal integration lengths T(min).

light rain could either be masked or falsely generated by noise within the radar equipment. In many studies, the value of P_0 is determined less by the measurements of very light rain but by the optimized fit of a rainfall rate distribution model to the full range of rainfall rates [47].

An example that reveals how the probability of rain occurrence changes with varying map sizes, S, is presented in Fig. 17. If a sufficiently long time interval is studied, the spatial variation in P_0 will exist due to orographic effects and microclimates. In this study, it is assumed that the 5 years of data are sufficiently long to estimate the long-term first-order statistics of rainfall rate. The P_0 is estimated through studying the proportion of 5 km cell with rainfall rates ($R > 0$) over the 5 year period. Fig. 17 shows significantly different rain probabilities between locations. For example, the rain occurrence pattern at Rennes is specific to this location which is at the end of the radar scan area and suffers from low data availability. As such, it exhibits larger than normal fluctuation than other chosen locations. The authors believe that the curves are valid for small surfaces (<100 km ^{2}) as they have been validated using 1 km spatial resolution scans from the British Isle-based radars. The proposed model gives sub-kilometer estimates but due to lack of data, their accuracies cannot be ascertained. In general, this difference poses a significant challenge in characterizing P_0 using a generic mathematical equation that encompasses three factors; L, T, and S. However, characterizing P_0 on a point-by-point basis avoids the problems introduced by averaging over inhomogeneous regions.

This is the difference between the approach proposed in this article and those reported elsewhere, where focus was on using the joint probability of rain to investigate the relationship between two locations, i.e., [48]. Those researchers estimated P_0 values for unmeasured location from measured ones.

According to [3], there is no easy physical way to determine P_0. In this article, P_0 has been studied from a grid point of view (with small area of $S = 5$ km $\times$ 5 km, the best estimate from the NIMROD radar systems for Europe) over a 5 year period with a range of spatial and temporal integration lengths at all locations. The results from the five studied locations are provided in this section. A mathematical equation has been proposed that gives a useful fit to the curves derived from the radar measurements

$$P_0(x) = 100 - b\,exp(cx^e) \tag{13}$$

where b, c, and e are model parameters which can be determined for each location and x denotes either spatial integration length L or temporal integration length T. The equation indicates that P_0 is constrained by two factors: L and T. Hence, the values of b, c, and e also exhibit variability for different spatial and temporal integration lengths.

The variation in P_0 with increasing integration length, both in space and time, together with the fitted curves, is shown in Fig. 18. P_0 is calculated using the same approach described in Section IV after integration. It shows that the value of P_0 also increases with an increase in the integration length. (The same information can be found in Tables VIII and IX.) It is evident (and logical) that P_0 values will drop close to 0 when

TABLE VIII
PROBABILITY OF RAIN AT FIVE LOCATIONS WITH DIFFERENT SPATIAL RESOLUTIONS RANGING FROM 5 TO 75 km, HERE $T = 15$ min

L (km)	5	10	15	20	25	35	40	45	50	55	65	75
Glasgow	26.2405	32.6411	38.9145	44.0160	47.2506	53.3291	56.7992	59.2708	63.2148	66.0124	68.3859	71.7900
Paris	9.4462	11.5436	13.9786	16.4933	18.1405	21.9438	23.2056	25.2637	27.0586	28.5131	31.5219	33.7558
Portsmouth	12.5768	16.4713	19.9222	23.1190	27.6801	33.7147	35.2840	38.3525	42.6886	44.3235	49.8689	53.7848
Rennes	15.9804	30.5540	36.4057	42.0667	48.7526	58.6829	60.3336	63.8205	65.2125	69.3576	75.0576	80.7791
Reims	10.6275	13.2886	15.8529	17.3246	19.4335	22.8025	24.6313	25.8012	28.8899	30.5064	32.5789	36.6841

TABLE IX
PROBABILITY OF RAIN AT FIVE LOCATIONS WITH DIFFERENT TEMPORAL RESOLUTIONS RANGING FROM 15 TO 120 min, HERE $L = 5$ km

T ($mins$)	15	30	45	60	75	90	105	120
Glasgow	26.2405	31.6275	35.1911	37.9202	40.2571	42.0518	44.0173	45.2660
Paris	9.4462	11.9088	13.8133	15.3373	16.7348	18.2439	19.2713	20.1700
Portsmouth	12.5768	15.5298	17.9649	19.7803	21.7471	23.1781	24.5094	25.7226
Rennes	15.9804	20.4940	23.6757	26.4001	28.7198	30.7892	32.5695	34.2906
Reims	10.6275	13.1766	15.0599	16.7234	18.2165	19.3508	20.3088	21.4758

TABLE X
EQUATION (13) FITTED PARAMETERS FOR A RANGE OF SPATIAL AND TEMPORAL INTEGRATION LENGTHS

	Space Domain		
L (km)	b	c	e
Glasgow	83.8814	−0.0353	0.803
Paris	94.3313	−0.0113	0.798
Portsmouth	91.0541	−0.0075	1.050
Rennes	109.2417	−0.0878	0.681
Reims	92.9020	−0.0103	0.824
	Time Domain		
T ($mins$)	b	c	e
Glasgow	90.4506	−0.0623	0.438
Paris	95.6420	−0.0113	0.582
Portsmouth	95.2737	−0.0215	0.512
Rennes	93.5656	−0.0228	0.573
Reims	96.5195	−0.0213	0.474

integration length approaches 0 or increases up to 100 when the integration length is long enough. Interestingly, Kundu and Siddani [49] found exactly the same empirical equations for the probability of rain occurrence based on rain gauge data.

The model parameter values of (13), for each location, are presented in Table X. The results show that the proposed P_0 expression gives good estimates throughout the whole range of integration lengths, especially in the time domain [see Fig. 18(b)]. This is because there are a large number of samples (5 years in total) for studying P_0 in the time domain but smaller number of samples in the space domain as only one location is focused on during each processing time.

VI. CONCLUSION

This article has presented the outcome of an extensive study of 5 years (2005–2009) of rain radar data spanning Oceanic climate in North-Western Europe. Four key characteristics of rainfall rate have been studied for a range of spatial and temporal integration lengths: 1) the annual statistical distribution; 2) the annual spatial correlation function; 3) the temporal correlation function; and 4) the point probability of rain/no rain.

It has been found that all the key characteristics of rain are strongly dependent on the spatial integration length (L) and temporal integration length (T). The results show that integration length has a significant impact on all key rain parameters owing to the high variability that rainfall intensity exhibits. This article proposes a new model that can be used to estimate the spatial and temporal correlations of rainfall rate at different integration lengths for any location in North-Western Europe. The method is capable of producing estimates at spatial integration lengths from $L = 5$ km to $L = 75$ km and temporal integration lengths from $T = 15$ min to $T = 1440$ min. This is critical for future simulation studies and will be highly applicable to satellite network research and planning.

The probability of rain occurrence has been shown to exhibit spatial variation over distances as short as 5 km. So far, no physical equation has been found that can combine the three factors (L, T, and S) to provide good estimates of P_0. An empirical model has been proposed in this article that can accurately estimate the P_0 value for a wide range of integration lengths: from $L = 5$ km to $L = 75$ km and between $T = 15$ min and $T = 1440$ min (1 day). The proposed model is valid when one of the spatial or temporal integration lengths is fixed for a fixed map size. In short, at least two factors should be constant when utilizing the proposed model to estimate P_0 values, and the combination is either {L, S} or {T, S}.

Finally, the results presented in this article show that rain field structure is not constant over large areas but vary from one location to another. This has also been partially demonstrated by other researchers such as in [6]. The statistical model proposed in this article yields more accurate results as rain characteristics have been studied at multiple locations for a wide range of integration volumes. In particular,

the proposed model significantly reduces the complexities and improves the accuracy of estimating rain characteristics and, hence, radio wave attenuation, for wide-area high-frequency communication network planning in North-Western Europe. This is because network planners and designers of physical layer fade mitigation techniques require knowledge of rain characteristics at smaller space and time scales than are typically available from radar or rain gauge measurements. Also, the prediction of quality of service (QoS) and the design of rain attenuation mitigation techniques rely on knowledge of short integration time of rain attenuation time series. This article has proposed a statistical model that can be used to estimate rain characteristics at finer scales that are required by rain field simulators to generate useful information such as rain-rate estimates for rain-induced attenuation statistics computation.

However, the proposed equations for modeling the rainfield characteristics are only valid for cases where either the spatial integration length or the temporal integration length is constant, while the other is changing. Therefore, our future work will focus on characterizing the rainfall fields in the space and time domains simultaneously.

ACKNOWLEDGMENT

REFERENCES

[1] R. K. Crane, *Electromagnetic Wave Propagation Through Rain*. Hoboken, NJ, USA: Wiley, 1996.

[2] A. D. Panagopoulos and J. D. Kanellopoulos, "On the rain attenuation dynamics: Spatial-temporal analysis of rainfall rate and fade duration statistics," *Int. J. Satell. Commun. Netw.*, vol. 21, no. 6, pp. 595–611, 2003.

[3] G. Yang, B. Gremont, D. Ndzi, and D. J. Brown, "Characterization of rain fields for UK satellite networks," in *Proc. Ka Broadband Commun., Navigat. Earth Observ. Conf.*, Oct. 2011.

[4] G. Yang, B. C. Gremont, L. Yang, M. E. Ibrahim, and L. Bai, "Space–time channel model for rain-affected communication networks," *IEEE Trans. Antenna Propag.*, vol. 67, no. 7, pp. 4768–4776, Jul. 2019. doi: 10.1109/TAP.2019.2907601.

[5] G. Yang, "Rainfall rate modelling for European satellite networks," Ph.D. dissertation, School Eng., Univ. Portsmouth, Portsmouth, U.K., 2016.

[6] L. Luini and C. Capsoni, "The impact of space and time averaging on the spatial correlation of rainfall," *Radio Sci.*, vol. 47, no. 3, pp. 1–10, Jun. 2012.

[7] B. Gremont, M. Filip, P. Gallois, and S. Bate, "Comparative analysis and performance of two predictive fade detection schemes for Ka-band fade countermeasures," *IEEE J. Sel. Areas Commun.*, vol. 17, no. 2, pp. 180–192, Feb. 1999.

[8] C. Enjamio, E. Vilar, A. Redano, F. P. Fontán, and D. Ndzi, "Experimental analysis of microscale rain cells and their dynamic evolution," *Radio Sci.*, vol. 40, no. 3, pp. 1–9, Jun. 2005.

[9] D. J. Seo, W. F. Krajewski, and D. S. Bowles, "Stochastic interpolation of rainfall data from rain gages and radar using cokriging: 1. Design of experiments," *Water Resour. Res.*, vol. 26, no. 3, pp. 469–477, 1990.

[10] D. A. Hughes, "Comparison of satellite rainfall data with observations from gauging station networks," *J. Hydrol.*, vol. 327, nos. 3–4, pp. 399–410, 2006.

[11] G. G. S. Pegram and A. N. Clothier, "High resolution space–time modelling of rainfall: The 'String of Beads' model," *J. Hydrol.*, vol. 241, nos. 1–2, pp. 26–41, 2001.

[12] K. S. Paulson, "Fractal interpolation of rain rate time series," *J. Geophys. Res., Atmos.*, vol. 109, no. D22, 2004.

[13] D. S. Wilks and R. L. Wilby, "The weather generation game: A review of stochastic weather models," *Progr. Phys. Geogr.*, vol. 23, no. 3, pp. 329–357, 1999.

[14] C. Onof, R. E. Chandler, A. Kakou, P. Northrop, H. S. Wheater, and V. Isham, "Rainfall modelling using Poisson-cluster processes: A review of developments," *Stochastic Environ. Res. Risk Assessment*, vol. 14, no. 6, pp. 384–411, 2000.

[15] T. Maseng and P. M. Bakken, "A stochastic dynamic model of rain attenuation," *IEEE Trans. Commun.*, vol. COMM-29, no. 5, pp. 660–669, May 1981.

[16] B. C. Gremont and M. Filip, "Spatio-temporal rain attenuation model for application to fade mitigation techniques," *IEEE Trans. Antennas Propag.*, vol. 52, no. 5, pp. 1245–1256, May 2004.

[17] A. Burgueno, E. Vilar, and M. Puigcerver, "Spectral analysis of 49 years of rainfall rate and relation to fade dynamics," *IEEE Trans. Commun.*, vol. 38, no. 9, pp. 1359–1366, Sep. 1990.

[18] L. Le Cam, "A stochastic description of precipitation," in *Proc. 4th Berkeley Symp. Math. Statist. Probab.* Berkeley, CA, USA: Univ. of California, Berkeley, vol. 3, 1961, pp. 165–186.

[19] J. Roldán and D. A. Woolhiser, "Stochastic daily precipitation models: 1. A comparison of occurrence processes," *Water Resour. Res.*, vol. 18, no. 5, pp. 1451–1459, 1982.

[20] B. C. Grémont and A. Tawfik, "Markov modelling of rain attenuation for satellite and terrestrial communications," in *Proc. 12th Int. Conf. Antennas Propag.*, 2003, pp. 369–373.

[21] P. S. P. Cowpertwait, "A spatial–temporal point process model of rainfall for the Thames catchment, UK," *J. Hydrol.*, vol. 330, nos. 3–4, pp. 586–595, 2006.

[22] M. Menabde, A. Seed, D. Harris, and G. Austin, "Self-similar random fields and rainfall simulation," *J. Geophys. Res., Atmos.*, vol. 102, no. D12, pp. 13509–13515, 1997.

[23] N. Jeannin, L. Féral, H. Sauvageot, L. Castanet, and J. Lemorton, "Statistical distribution of the fractional area affected by rain," *J. Geophys. Res.*, vol. 113, no. D21, Nov. 2008. doi: 10.1029/2008JD009780.

[24] T. L. Bell, "A space-time stochastic model of rainfall for satellite remote-sensing studies," *J. Geophys. Res.*, vol. 92, no. D8, pp. 9631–9643, Aug. 1987.

[25] M. Valeria, R. Fabio, N. Francesco, L. Federico, and B. Luca, "Study of the rainfall dependence structure using radar and rain gauge data," in *Proc. Int. Workshop Adv. Stat. Hydrol.*, Tormina, Italy, May 2010.

[26] N. Jeannin, "A space-time channel model for simulations on continental satellite coverages: Overview of the modeling and potentiality for adaptive resource management optimization," in *Proc. ESA Propag. Workshop*, Noordwijk, The Netherlands, Dec. 2008.

[27] B. W. Golding, "Nimrod: A system for generating automated very short range forecasts," *Meteorolog. Appl.*, vol. 5, no. 1, pp. 1–16, 1998.

[28] K. S. Paulson, "Trends in the incidence of rain rates associated with outages on fixed links operating above 10 GHz in the southern United Kingdom," *Radio Sci.*, vol. 45, no. 1, pp. 1–9, Feb. 2010. doi: 10.1029/2009RS004193.

[29] D. L. Harrison, S. J. Driscoll, and M. Kitchen, "Improving precipitation estimates from weather radar using quality control and correction techniques," *Meteorolog. Appl.*, vol. 7, no. 2, pp. 135–144, 2000.

[30] M. Filip and E. Vilar, "Optimum utilization of the channel capacity of a satellite link in the presence of amplitude scintillations and rain attenuation," *IEEE Trans. Commun.*, vol. 38, no. 11, pp. 1958–1965, Nov. 1990.

[31] K. S. Paulson and X. Zhang, "Simulation of rain fade on arbitrary microwave link networks by the downscaling and interpolation of rain radar data," *Radio Sci.*, vol. 44, no. 2, pp. 1–10, Apr. 2009.

[32] K. S. Paulson, L. Luini, N. Jeannin, B. C. Gremont, and R. J. Watson, "A review of channel simulators for heterogeneous microwave networks," *IEEE Antennas Propag. Mag.*, vol. 55, no. 5, pp. 118–127, Oct. 2013.

[33] B. Kedem and L. S. Chiu, "On the lognormality of rain rate," *Proc. Nat. Acad. Sci. USA*, vol. 84, no. 4, pp. 901–905, Feb. 1987.

[34] *Characteristics of Precipitation for Propagation Modelling*, document ITU-R Rec. 837-7, P Series, Geneva, Switzerland, 2017.

[35] K. Morita and I. Higuti, "Prediction methods for rain attenuation distributions of micro and millimetre waves," *Rev. Electron. Commun. Lab.*, vol. 24, nos. 7–8, pp. 651–668, 1976.

[36] R. Berndtsson, "Temporal variability in spatial correlation of daily rainfall," *Water Resour. Res.*, vol. 24, no. 9, pp. 1511–1517, 1988.

[37] A. Basist, G. D. Bell, and V. Meentemeyer, "Statistical relationships between topography and precipitation patterns," *J. Climate*, vol. 7, no. 9, pp. 1305–1315, 1994.

[38] H. W. T. Maat, E. J. Moors, R. W. A. Hutjes, A. A. M. Holtslag, and A. J. Dolman, "Exploring the impact of land cover and topography on rainfall maxima in The Netherlands," *J. Hydrometeorology*, vol. 14, no. 2, pp. 524–542, 2013.

[39] B. Johansson and D. Chen, "The influence of wind and topography on precipitation distribution in Sweden: Statistical analysis and modelling," *Int. J. Climatol.*, vol. 23, no. 12, pp. 1523–1535, 2003.

[40] H. Fukuchi, "Correlation properties of rainfall rates in the United Kingdom," *IEE Proc. H Microw., Antennas Propag.*, vol. 135, no. 2, pp. 83–88, Apr. 1988.

[41] T. Manabe, H. Kobayashi, T. Ihara, and Y. Furuhama, "Spatial correlation coefficients of rainfall intensity inferred from statistics of rainfall intensity and rain attenuation," *Annales Télécommun.*, vol. 41, nos. 9–10, pp. 463–469, 1986.

[42] Z. Şen and Z. Habib, "Monthly spatial rainfall correlation functions and interpretations for Turkey," *Hydrolog. Sci. J.*, vol. 46, no. 4, pp. 525–535, 2001.

[43] P. V. Mandapaka, W. F. Krajewski, G. J. Ciach, G. Villarini, and J. A. Smith, "Estimation of radar-rainfall error spatial correlation," *Adv. Water Resour.*, vol. 32, no. 7, pp. 1020–1030, 2009.

[44] C. Capsoni, E. Matricciani, and M. Mauri, "Profile statistics of rain in slant path as measured with a radar," *Alta Frequenza*, vol. 54, no. 2, pp. 50–57, 1985.
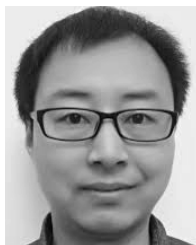
[45] G. Hendrantoro, Indrabayu, T. Suryani, and A. Mauludiyanto, "A multivariate autoregressive model of rain attenuation on multiple short radio links," *IEEE Antennas Wireless Propag. Lett.*, vol. 5, no. 1, pp. 54–57, Dec. 2006.

[46] G. I. Taylor, "Statistical theory of turbulence," *Proc. Roy. Soc. London A, Math., Phys. Eng. Sci.*, vol. 151, no. 873, pp. 421–444, Sep. 1935.

[47] Y. Otsu, Y. Takahashi, and T. Kozu, "Simultaneous occurrence probabilities of rainfall among nine locations in Japan," *Electron. Lett.*, vol. 22, no. 18, pp. 937–938, Aug. 1986.

[48] F. Barbaliscia, G. Brussaard, and A. Paraboni, "Characteristics of the spatial statistical dependence of rainfall rate over large areas," *IEEE Trans. Antennas Propag.*, vol. 40, no. 1, pp. 8–12, Jan. 1992.

[49] P. K. Kundu and R. K. Siddani, "Scale dependence of spatiotemporal intermittence of rain," *Water Resour. Res.*, vol. 47, no. 8, 2011.

Boris Christian Gremont was born in 1969. He received the bachelor's degree (Hons.) in engineering and the Ph.D. degree in electrical electronic engineering from Coventry University, U.K., in 1994 and 1998, respectively.

He was appointed as a Senior Lecturer at the Department of Electronics and Computer Engineering, University of Portsmouth, Portsmouth, U.K. He was also involved in the European COST 280 action "Propagation Impairment Mitigation for Millimeter Wave Radio Systems" and he also contributed to the UK's RAINMAP project (Fractal Rain Modeling for Millimeter-Wave Propagation). He jointly initiated this research but past away before it was fully completed.

Kevin Paulson is currently a Senior Lecturer with the School of Engineering and Computer Science, University of Hull, Hull, U.K. He was the first in the world to find evidence of the effects of climate change on radio telecommunications and was the co-author of the UK's Climate Change Evidence Report 2017. His main area of expertise is in stochastic signal processing, which he is applying to medical engineering and radio propagation. More recently, he has focused on the analysis of ECG and EEG signals measured with ambulatory systems.

Dr. Paulson is a member of the ITU-R UK Study Group 3 coordinating propagation studies.

Guangguang Yang received the Diploma degree (Hons.) from Xinxiang College, Xinxiang, China, in 2008, and the bachelor's degree (Hons.) and Ph.D. degree in electronic engineering from the University of Portsmouth, Portsmouth, U.K., in 2010 and 2016, respectively.

His current research interests include earth–space, terrestrial and wideband propagation, and satellite communications.

Misha Filip received the Ph.D. degree in digital satellite communications from the University of Portsmouth, Portsmouth, U.K., in 1991.

He worked in the industry for a number of years before becoming a Principal Lecturer and the Head of the School of Engineering, University of Portsmouth. He worked on a number of EU COST Actions and took a leading role in COST 280 on propagation impairment mitigation for millimeter-wave radio systems. His research interests include satellite communications, digital wellbeing, and smart systems for manufacturing warehousing.

David L. Ndzi received the B.Sc. degree (Hons.) in electronics and mathematics from Keele University, Keele, Newcastle, U.K., in 1994, and the Ph.D. degree in telecommunications from the University of Portsmouth, Portsmouth, U.K., in 1998.

He was a Principal Lecturer and the Faculty of Technology International Coordinator at the University of Portsmouth until 2017. He is currently the Head of Computing at the University of the West of Scotland. His research interests include wireless sensor networks and mesh networks for applications in environmental monitoring and prediction, behavioral economics, security, building control, and energy management.

Abdul-Hadi Al-Hassani received the bachelor's degree from the University of Basra, Basrah, Iraq, the master's degree from the University of Bradford, Bradford, U.K., and the Ph.D. degree from Loughborough University, Loughborough, U.K.

He is currently the General Director of the Basra Centre for Strategic Studies and also the Chancellor of the Iraq University College Basrah, Basrah. His research interests include environmental monitoring and applications in construction and disaster prevention.